IEEE Access
Multidisciplinary | Rapid Review | Open Access Journal

Received March 28, 2018, accepted May 11, 2018, date of publication May 16, 2018, date of current version June 29, 2018.

Digital Object Identifier 10.1109/ACCESS.2018.2837083

Evaluation on EM Scattering Properties From a Wind Farm by an Efficient High-Frequency Method

WEI YANG, (Member, IEEE), CONGHUI QI, AND YUYUE ZHANG
School of Electronic Science and Engineering, University of Electronic Science and Technology of China, Chengdu 611731, China

Corresponding author: Conghui Qi (chqi@uestc.edu.cn)

This work was supported in part by the National Defense Equipment Pre-Research Foundation of China under Grant 14YY170803A, in part by the Fundamental Research Funds for the Central Universities under Grant ZYGX2016KYQD128, and in part by the China Postdoctoral Science Foundation under Grant 2016M592655.

ABSTRACT In order to study the dynamic signature from a wind farm composed of massive wind turbines, a high-frequency model of electromagnetic scattering is developed by combining a shooting and bouncing ray and the array synthesis technique. With the help of image theory and some modifications, the ground effects due to a dielectric rough ground are accounted whereas without modeling physically the infinite ground. Thus, the proposed method can be used to effectively simulate the massive required scattering data under a minimal computational cost for the Doppler analysis of the full-size rotating wind turbines and radar imaging of a wind farm.

INDEX TERMS Doppler effect, SAR imaging, shooting and bouncing rays, image theory, wind farm.

I. INTRODUCTION

Wind power is certainly one of the most economical and sustainable energy resources with increasing globally at a rate of about 20 percent annually. Its installations interfere with existing electronic equipment for surveillance, navigation, communications, etc. [1], [2]. The blade flash of rotating turbine can interfere with radar detection of moving targets and give rise to cross-range artifacts in high-resolution synthetic aperture radar (SAR) imaging. It is therefore an emerging issue to assess electromagnetic environment impacts of wind farm.

As for the assessment of the wind farm, in aspect of commercial cost and convenience, electromagnetic (EM) simulation has more advantages than the EM measurement. Due to the tremendous amount of computational costs associated with the large structure of wind turbine and farm, the full-wave solutions, such as multilevel fast multipole algorithm (MLFMA) [3], can become impractical and intractable. Existing simulation cases mainly focused on the scaled model [4], [5] or on the simplified free-space model [6], [7] discussed this problem of wind turbine on a flat (not rough) ground. Meanwhile, instead of the single wind turbine, none of publications has discussed the EM simulation technique for the wind farm problem composed of massive wind turbines.

Different from the previous methods, this paper aims to assess the scattering properties of a wind farm on dielectric rough surface, such as an offshore wind farm on sea surface. An efficient high-frequency model is developed to analyze the electromagnetic scattering from massive wind turbines. It can not only account the ground effects whereas without modeling the infinite ground, but also simulate the scattering of the massive turbines to avoid the exhausting efforts of integrated simulation of wind farm. Therefore, this model is an effective tool to investigate dynamic signature from a wind farm. Then, based on the proposed method, the massive scattering data are produced and then used to analyze the dynamic signature of rotating turbines according to the signal processing. This work benefits to study the scattering mechanism and further to explore the mitigation interference techniques.

II. THE PROPOSED METHOD

For this kind of composite target-ground problem, the high-frequency approximation has better potential to simulate it with reasonable accuracy while providing physical insights.

A. TURBINE ELEMENT ON GROUND

The multiple bounces of the EM wave between the surfaces of turbine as well as between turbine and ground are handled by shooting and bouncing rays (SBR) [8]. However, the main scattering contributions are from the four components as shown in Fig. 1, called as the 'four-path' model [9], [10]. Since the axis of turbine is almost vertical, the ray-bounces between the turbine and its below-ground are limited, except these four paths, other scattering components are ignored [11]. On the other hand, it is not practical to physically model the nearly infinite rough ground surface. Otherwise, an enormous number of rays are required to capture all the multiple bounces between ground and turbine, which drastically increases memory requirement and CPU time.

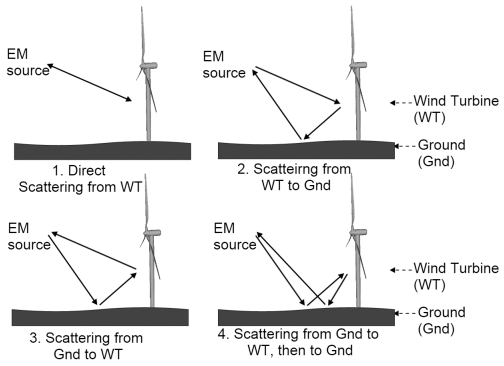

FIGURE 1. Four scattering components from a wind turbine in the presence of ground.

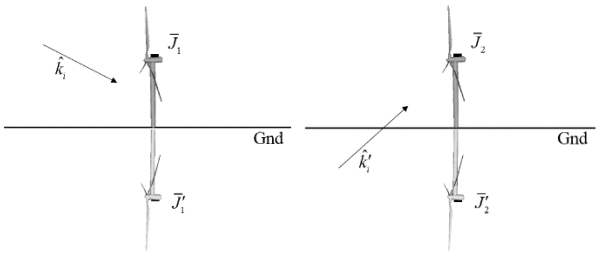

FIGURE 2. Image theory for the four scattering components. (a) Imaged induced electric current. (b) Imaged incident plane wave.

The four components can be obtained with the help of two images: an imaged induced electric current and an imaged incident plane wave as illustrated in Fig. 2. Firstly, the ground is considered as the perfectly electrically conducting (PEC) flat plane. The original incident magnetic field at source point $\bar{r}'$ is $\bar{H}(\bar{r}')= \hat{h}_i e^{-jk\hat{k}_i\cdot\bar{r}'}$, where $\hat{h}_i$ is the polarization direction, k is the wavenumber, $\hat{k}_i(k_x, k_y, k_z)$ is the direction of incident wave determined by the incident angle (θ,φ). If the original induced current on the turbine is $\bar{J}(j_x, j_y, j_z)$, then its imaged electric current is $\bar{J}'(j_x', j_y', j_z')$, $j_x' = -j_x$, $j_y' = -j_y$, $j_z' = j_z$. In Fig. 2(a), the induced electric current $\bar{J}_1$ and its imaged current $\bar{J}_1'$ correspond to the first and second scattering components in the Fig. 1.

For the imaged incident plane wave due to the plane, the imaged incident wave vector is $\hat{k}_i'(k_x', k_y', k_z')$, $k_x' = k_x$, $k_y' = k_y$, $k_z' = -k_z$ in Fig. 2(b), the induced electric current $\bar{J}_2$ and its imaged current $\bar{J}_2'$ correspond to the third and fourth scattering components in the Fig. 1.

Then, to handle the rough dielectric ground, the two aforementioned images have to be modified by the factor Γ for dielectric case and the coefficient ρ_s for rough case.

For the imaged electric current:

$$\bar{J}' = \Gamma\cdot\rho_s\cdot\bar{J}\left(-j_x, -j_y, j_z\right) \tag{1}$$

For the imaged incident plane wave:

$$\bar{H}'\left(\bar{r}'\right) = \Gamma\cdot\rho_s\cdot\hat{h}_i e^{-jk\hat{k}_i'\cdot\bar{r}'} \tag{2}$$

where ρ_s is determined by [12]

$$\rho_s = \begin{cases} \exp\left[-2\,(2\pi\tau)^2\right] & 0 \le \tau \le 0.1 \\ 0.812537/\left[1+(2\pi\tau)^2\right] & \tau > 0.1 \end{cases} \tag{3}$$

where $\tau = \sigma_h\cos\theta/\lambda$, λ is EM wavelength, σ_h is the standard deviation of the ground surface elevation. In addition, the parameter Γ in (1) and (2) is given by

$$\Gamma_{HH} = \frac{\sqrt{\varepsilon_r - \sin^2\theta} - \cos\theta}{\sqrt{\varepsilon_r - \sin^2\theta} + \cos\theta} \tag{4.a}$$

$$\Gamma_{VV} = \frac{\varepsilon_r\cos\theta - \sqrt{\varepsilon_r - \sin^2\theta}}{\varepsilon_r\cos\theta + \sqrt{\varepsilon_r - \sin^2\theta}} \tag{4.b}$$

where ε_r is the relative dielectric constant of ground, HH and VV donate horizontal-horizontal (HH) polarization and vertical-vertical (VV) polarization, respectively. And θ is the scattering (or incident) angle for Γ in (1) (or (2)). The modified factor is related to the EM polarizations and incident/scattering angles.

Compared with the path 1 in the Fig. 1, the phase delays for other three paths have been automatically accounted into the above two image processes. With these treatments, only the ray tubes illuminating the wind turbine are required and the physical modeling of the ground is avoided. There are only two ray-tracing processes to obtain four components. The target-ground problem is then transferred to the free-space problem. Thus, the memory consumption is almost same as the case of the target in free space, and the CPU time is about twice that of the free-space problem.

B. ARRAY OF TURBINES

Since the wind farm is an array of turbines, it is important to analyse the overall scattering from this array. Generally, the spacing between two adjacent turbines is very large versus EM wavelength (more than thousands of lambda). The large spacing leads to be reasonable to ignore the EM coupling among turbines. For a wind farm composed of M∗N wind turbines and its arbitrary location $\bar{r}_{mn}$ of the *mn*-th turbine

element, based on the antenna array synthesis [13], the total scattered field is computed by

$$\bar{E}_s^{total}(\bar{r}) = \bar{E}_s(\bar{r}) \cdot \left(\Sigma_{m=1}^{M} \Sigma_{n=1}^{N} e^{jk\left(\hat{r}-\hat{k}_i\right)\cdot \bar{r}_{mn}} \right) \quad (5)$$

$\hat{r}$ denotes the scattering direction. The former and latter terms in (5) are turbine element scattering and array factor, respectively. Therefore, the proposed method only needs to model the single turbine at different rotation status and different incident angles, which can avoid the exhausting efforts of integrated simulation of turbine array. So, it can minimize the required computational resources.

The quasi-static electromagnetic simulation is used to obtain the scattering data of the dynamic wind turbine driven by a certain wind speed. Since the maximum linear velocity of rotating blades is much smaller than light speed, the scattered field generated from wind turbine at a moment is similar to the ones generated from the motionless targets which dwell at its trajectory. Finally, the time-varying returns are obtained at the different moments with different random states of blades.

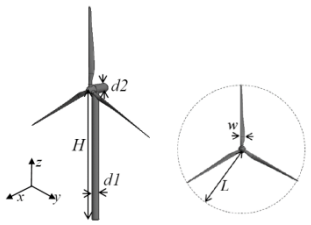

Tower height:	H=70m
Tower diameter:	d1=3.9m
Rotor diameter:	d2=4.8m
Blade length:	L=45.1m
Blade width:	w=1.6m

FIGURE 3. A generic wind turbine.

To assess the accuracy and efficiency of this method, a generic real-size three-blade wind turbine (Web link to access: https://grabcad.com/library/wind-turbine–4/files) on a ground is modelled and its parameters are shown in Fig. 3. The proposed method is applied to simulate the bi-static scattering of this turbine on the flat dielectric ground plane with $\varepsilon_r = 4.6 - j0.01$, at incident angle (45°, 0°) at 100MHz frequency. Fig. 4 shows that there is fairly good agreement between the bi-static scattering results obtained by the proposed method and half-space MLFMA by a commercial software FEKO [14] in *xoz* cut, where FEKO-MLFMA can provide the rigorous reference data. It is observed that the proposed method is sufficient to capture most of the key EM signatures of the large-scale wind turbine. It is no doubt that the more accurate results can be obtained at higher frequencies.

To minimize computation time without any loss in model fidelity, we used only 2145 triangular facets for the model in our method while 149,742 facets were used for the model in FEKO-MLFMA. The computational costs are as follows: FEKO-MLFMA used 1.14GigaBytes (GB) of peak RAM and took 5.8 hours. Instead, the proposed method used 4.3MegaBytes (MB) and 0.3 minutes for this target-ground composite scattering problem whereas the costs of 4.3MB and 0.17 minutes for an isolated wind turbine without ground.

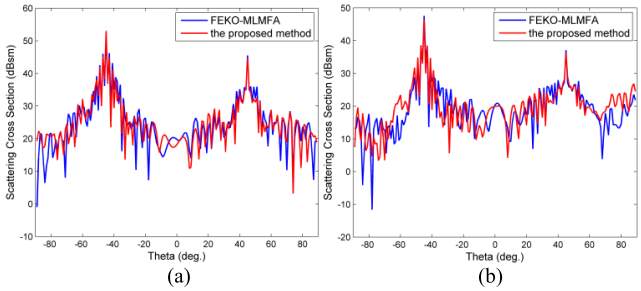

FIGURE 4. Comparison of bi-static scattering of a wind turbine on a dielectric ground. (a) HH polarization. (b) VV polarization.

III. NUMERICAL RESULTS

The simulation is extended to some realistic cases. Supposed that a rectangle wind farm composed of 48 (M = 8, N = 6) equidistant wind turbines on a dielectric rough ground with the relative dielectric constant $\varepsilon_r = 4.6 - j0.01$, and the standard deviation of ground $\sigma_h = 0.01$m, where the turbine location is $\bar{r}_{mn} = [(m-1)R_x, (n-1)R_y, 0]$, the turbine spacing is assumed to be Rx in x direction and Ry in y direction. The EM wave is working at 3GHz (S-band).

A. DOPPLER FEATURE ANALYSIS

We study the Doppler features [15], [16] of EM scattering from a full-size wind turbine with rotating blades in the presence of ground. For instance, the wind turbine rotates at 12rpm which gives a maximum blade tip speed of 56.7m/s. The blade rotation driven by wind could cause a significant change in scattered fields. To perform the dynamic simulation, the backscattered data are collected for each snapshot of the turbine blades, in 0.02° increments, over the duration of 2.5 seconds. For different snapshot, the turbine is reconstructed by the two part of static tower and rotating blades. It is noted that the three-blade turbine is a 120° symmetry of the structure, and it includes one complete evolution of the turbine blades.

The data are simulated by the proposed method, and then the Doppler spectrograms processed by using the short-time Fourier transform with a time window of 0.0356seconds (128 sampling points) for the rotation rate of 12rpm.

The presence of ground introduces complexity to the returned signal due to the target-ground interactions in addition to the direct return to the target. The turbine is assumed to be at a 90°yaw angle with respect to the radar. Simulations are performed to investigate the time-varying Doppler features that arise from target-ground interactions. The strong zero-Doppler features are from the static tower. With ground interactions, new Doppler tracks in addition to the strong flashes and weak tip halos are expected in the time-dependent Doppler spectrum, as shown in Fig. 5(a). Because of the different thicknesses of two sides of blades, the spectrum energy of moving towards the source is stronger than that of moving backwards the source. And the tracks that arise from ground effects are identified and interpreted in Fig. 5(b). The spectrums caused by multipath between

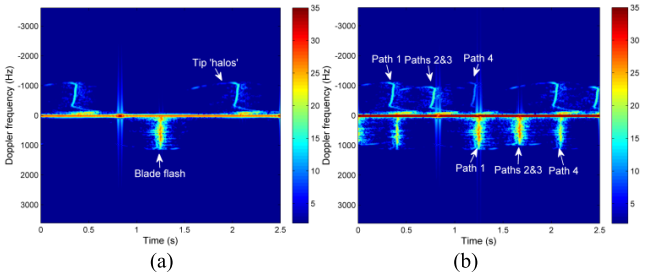

FIGURE 5. Ground effects under the incidence of 60°, HH polarization. (a) Without ground. (b) With ground.

turbine and ground occur in time after the direct flash (path 1) due to propagation path delays. And the bounce (path 2) from ground to turbine is identical with the bounce from turbine to ground (path 3). Meanwhile, the high-order bounce (path 4) gives rise to weak flash. These phenomena are coincident with the results of some experiments in [4].

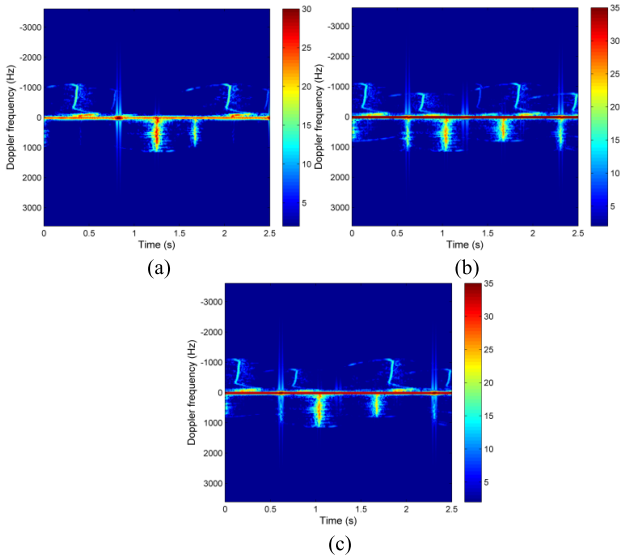

FIGURE 6. Spectrograms of rotating turbine. (a) $\theta = 60°$, VV polarization. (b) $\theta = 45°$, HH polarization. (c) $\theta = 45°$, VV polarization.

Next, we generated more simulations at two incidences. The maximum Doppler from the moving wind turbines are theoretically 1.13kHz. From the Fig. 6, it is found that the ground effects are very weak and the scattering of path 1 is dominant for the result of VV polarization at 60° incidence. The physical mechanism can be explained as follows: since the VV polarized EM wave is transmitted through a dielectric ground with no reflection at a particular angle, called as Brewster angle, it means that the contributions of paths 2∼4 are very weak. For the ground of $\varepsilon_r = 4.6 - j0.01$, the reflection ratio is very small near 63^o incidence. And this phenomenon does not occur in the case of VV polarization at 45°. From these spectrograms, the rotating turbine blades can interfere with the EM detection of moving targets, and ground effects make it more sophisticated.

Next, we generated the SAR image from a dynamic wind farm, the incident is from at edge-on direction. The sensor

TABLE 1. Basic radar parameters.

Scene size	3.2km*5km
Resolution	2m
Sampling Points	1600*2500
Radar Sensor Speed	150m/s
Radar Range	20km
Frequency Bandwidth	75MHz
Angular width in Azimuth	1.4333°

and wind farm parameters are listed in Table 1. The duration of radar data collection is about 3.33seconds. For a dynamic turbine with a random initial status, it includes 1600 individual time snapshots during this duration and corresponds to a rotation of 0.15° per time step. Each snapshot of pre-defined rotating portion can generate 2500 backscattering data at different frequencies within radar bandwidth. For this farm, each turbine has its individual initial status. So, the radar database for the wind turbine at a range of frequencies and angles were simulated and stored by our proposed method. Once the database was computed for one turbine, the returns from all the wind turbines were combined coherently to form the total radar return from the wind farm according to the (5). Finally, the EM simulation from the wind farm was post-processed using a SAR imaging algorithm [17], [18].

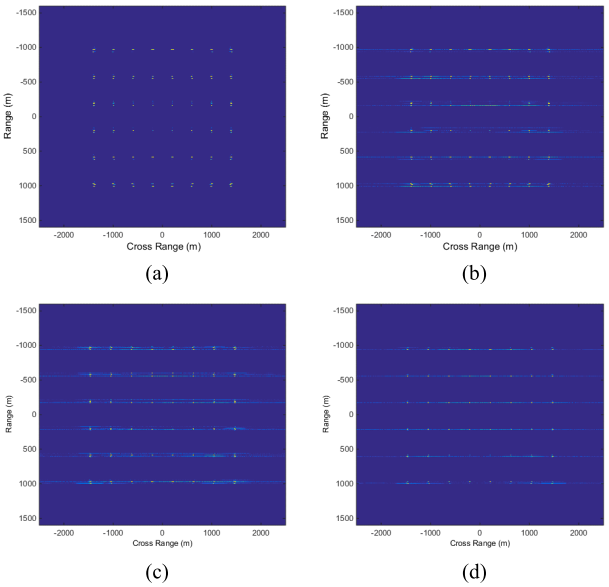

FIGURE 7. SAR image of a wind farm. (a)-(c) HH polarization, (d) VV polarization. (a) $\theta = 45°$, stationary turbines. (b) $\theta = 45°$, dynamic turbines. (c) $\theta = 60°$, dynamic turbines. (d) $\theta = 60°$, dynamic turbines.

Firstly, an example SAR image of the stationary scene is show in Fig. 7(a), where the blades are supposed to be static (or: quasi-static). The wind turbines are stationary there are no artifacts generated from them in the SAR image.

Secondly, we study the dynamic signature of rotating blades. The moving blades generate Doppler features, leading to cross-range artifacts in the SAR image of the scene, as shown in Fig. 7(b)-(d). There artifacts run along the cross

range dimension and can extend beyond the physical location of the wind farm in the SAR images. The Doppler from the wind turbines blades depends on the position of the blades and as the wind turbines blades rotate these artifacts keep changing in amplitude. In addition, the moving blades may give rise to cross-range artifacts in high-resolution SAR imaging. The VV polarized wave can reduce the interference effect from ground and avoid artifact in SAR, and HH wave is more serve. Generally, it will affect the detection of the interesting targets, such as car and ship. Especially for the target located within the cross-range location of the wind turbine would be affected since it would be quite difficult to discern the target from the rapidly changing wind turbine artifacts.

Even the computational cost varies from different incident angles and the states of wind turbine, the RAM and CPU time for single incidence at S-band are about 51MB, and 6.1 minutes, respectively. It takes about 38hours to generate all backscattering data required on a LINUX platform with Intel®CoreTM E5-4650 2.70GHz processors (32 Cores). Therefore, it shows that the proposed method has a potential to solve the EM scattering problem of wind farm.

IV. CONCLUSIONS

An effective high-frequency model has been developed to analyze the EM scattering problem from a wind farm composed of massive turbines, and capture the most scattering signatures of wind farm with very low computational costs. Because of the limitation of usage of the image theory, this model fails to solve the more complex case if its underlying ground is an irregular surface. However, the proposed method is well-suited for simple estimation of a wind farm on a flat or randomly rough surface, such as a typical sea wind farm scenario. Understanding the features of the clutter is a first step towards mitigation measures. Therefore, this work is useful to assess the impacts and mitigate wind farm interference to other electronic systems.

ACKNOWLEDGMENT

The authors would acknowledge Dr. Chao-Fu Wang, Temasek Laboratories, National University of Singapore, for his some valuable suggestions to improve this paper.

REFERENCES

[1] H. Ling *et al.*, "Assessment of offshore wind farm effects on sea surface, subsurface and airborne electronic systems," Dept. Energy, Univ. Texas Austin, Austin, TX, USA, Final Rep. DE-EE0005380, 2013.
[2] I. Angulo *et al.*, "Empirical evaluation of the impact of wind turbines on DVB-T reception quality," *IEEE Trans. Broadcast.*, vol. 58, no. 1, pp. 1–9, Mar. 2012.
[3] S. Järvenpää and P. Ylä-Oijala, "Multilevel fast multipole algorithm with global and local interpolators," *IEEE Trans. Antennas Propag.*, vol. 62, no. 9, pp. 4716–4725, Sep. 2014.
[4] Y. Zhang, A. Huston, R. D. Palmer, R. Albertson, F. Kong, and S. Wang, "Using scaled models for wind turbine EM scattering characterization: Techniques and experiments," *IEEE Trans. Instrum. Meas.*, vol. 60, no. 4, pp. 1298–1306, Apr. 2011.
[5] Y. An, D. Wang, and R. S. Chen, "A fast numerical algorithm for calculating electromagnetic scattering from an object above a rough surface," *Electromagnetics*, vol. 33, no. 1, pp. 10–22, 2013.
[6] D. Jenn and C. Ton, "Wind turbine radar cross section," *Int. J. Antennas Propag.*, vol. 2012, Dec. 2012, Art. no. 252689, doi: 10.1155/2012/252689.
[7] A. Naqvi, N. Whitelonis, and H. Ling, "Doppler features from wind turbine scattering in the presence of ground," in *Proc. Int. Symp. Antennas Progag. Soc. Res. Lett.*, vol. 35, Jul. 2012, pp. 1–2.
[8] W. Yang, C. Y. Kee, and C.-F. Wang, "Novel extension of SBR–PO method for solving electrically large and complex electromagnetic scattering problem in half-space," *IEEE Trans. Geosci. Remote Sens.*, vol. 55, no. 7, pp. 3931–3940, Jul. 2017.
[9] H. T. Anastassiu, "A closed form, physical optics expression for the radar cross section of a perfectly conducting flat plate over a dielectric half-space," *Radio Sci.*, vol. 38, no. 2, pp. 10-1–10-13, 2003.
[10] Y. Zhao, M. Zhang, Y.-W. Zhao, and X.-P. Geng, "A bistatic SAR image intensity model for the composite ship–ocean scene," *IEEE Trans. Geosci. Remote Sens.*, vol. 53, no. 8, pp. 4250–4258, Aug. 2015.
[11] S. Kashyap and A. Louie, "RCS of an object inclined to a ground plane," *Microw. Opt. Technol. Lett.*, vol. 18, no. 1, pp. 50–54, 1998.
[12] Y. Wang, X. J. Xu, "On wideband radar signature simulation of ships over sea surface," (in Chinese), *Acta Aeronaut. ET Astronaut. Sinica*, vol. 30, no. 2, pp. 337–342, 2009.
[13] M. T. Ma, *Theory and Application Antenna Arrays*. Hoboken, NJ, USA: Wiley, 1974.
[14] *FEKO Suite 7.0*, EM Softw. Syst.-S.A., Stellenbosch, South Africa, May 2014. [Online]. Available: http://www.feko.info
[15] C. J. Li, R. Bhalla, and H. Ling, "Investigation of the dynamic radar signatures of a vertical-axis wind turbine," *IEEE Antennas Wireless Propag. Lett.*, vol. 14, pp. 763–766, 2015.
[16] R. Nepal, J. Cai, and Z. Yan, "Micro-Doppler radar signature identification within wind turbine clutter based on short-CPI airborne radar observations," *IET Radar, Sonar Navigat.*, vol. 9, no. 9, pp. 1268–1275, Dec. 2015.
[17] C. J. Li, S. T. Yang, and H. Ling, "*In-situ* ISAR imaging of wind turbines," *IEEE Trans. Antennas Propag.*, vol. 64, no. 8, pp. 3587–3596, Aug. 2016.
[18] J. W. Dai and Y.-Q. Jin, "Imaging and reconstruction of a 3D complex target using downward-looking step-frequency radar," in *Proc. 9th Int. Symp. Antennas Propag. EM Theory (ISAPE)*, Guangzhou, China, Nov. 2010, pp. 892–896.

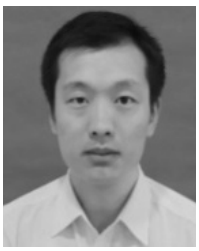

WEI YANG (M'12) was born in Suining, Sichuan, China, in 1984. He received the B.S. degree from Sichuan University, Chengdu, China, in 2007, and the Ph.D. degree from the University of Electronic Science and Technology of China, Chengdu, in 2012. From 2012 to 2013, he was with Huawei Technologies Company as a Research Engineer to work on next-generation (5G) wireless communication. From 2014 to 2016, he was with Temasek Laboratories, National University of Singapore, as a Research Scientist. He is currently an Assistant Professor with the School of Electronic Science and Engineering, University of Electronic Science and Technology of China.

He has published over 25 journal papers and holds two patents. His research interests include antenna design, computational electromagnetics, radar imaging, and signal processing.

CONGHUI QI was born in Shijiazhuang, Hebei, China, in 1987. She received the B.S. and Ph.D. degrees from the University of Electronic Science and Technology of China (UESTC), Chengdu, in 2009 and 2015, respectively. She currently holds a post-doctoral position at the School of Electronic Science and Engineering, UESTC. Her research interests include computational electromagnetics and radar signal processing.

YUYUE ZHANG was born in Jinan, Shandong, China, in 1996. He received the B.S. degree from the University of Electronic Science and Technology of China in 2016, where he is currently pursuing the M.S. degree. His research interests include rough surface scattering.